

Residual Stress in Brazing of Submicron Al_2O_3 to WC-Co

T. Grunder, A. Piquerez, M. Bach, and P. Mille

(Submitted May 5, 2015; in revised form March 30, 2016; published online June 10, 2016)

This study evaluated the residual stresses induced by brazing and grinding submicron Al_2O_3 , using different methods. Energy dispersive x-ray spectrometry analysis (EDX) of 72Ag-Cu filler and filler/WC-Co interface showed evidence of atomic diffusion and possible formation of titanium oxide layers between the joint and the bonding materials. An analytical model supported by the finite element method (FEM) based on strain determination due to the difference in variation of thermal expansion was used to assess the stress distribution at the coupling interface and in bulk materials. The model took into account the evolution of the Young's modulus and of the thermal expansion with temperature. The model could be used to follow strain and stress evolutions of the bonded materials during the cooling cycle. The maximum stress rose above -300 MPa at the center of the $100 \times 100 \times 3$ mm ceramic plates. The residual stresses on the external surface of ceramic were investigated by x-ray diffraction (XRD) and indentation fracture method (IFM). After brazing and grinding the plate, the principal stresses were 128.1 and 94.9 MPa, and the shear stress was -20.1 MPa. Microscopic examination revealed grain pull-out promoted by the global residual stresses induced by the brazing and grinding processes. The surface stresses evaluated by the different methods were reasonably correlated.

Keywords brazing, residual stress, submicron alumina

1. Introduction

On one hand, the brazing of engineering ceramics opened the field for many new applications like the bonding of cutting inserts for tools and of electronic compounds in high vacuum systems (Ref 1). This means the assembly has to resist to high mechanical loading and durability through cycles and preserve hermeticity for a long working time (Ref 2, 3). On the other hand, the ceramic manufacturing methods have been improved to provide higher mechanical properties, such as hardness in the case of submicron alumina (Ref 4). However, some difficulties appear in the ceramic-metal assembly to keep their integrity due to high residual stress that appears after being coupled by brazing. The main difficulty in joining ceramic to metal is due to the coefficient of thermal expansion (CTE) mismatch between these two materials that leads to residual stress during the cooling. Usually, the adjustment of the CTE is the best way to reduce this stress. The use of a ductile joint could also play a key role in the relaxation of part of the residual stress by plastic deformation (Ref 5, 6).

The field of application of this work is the design of new ceramic cutting tools for the machining of wood-based materials (Ref 7). Ceramic is first bonded on a substrate, like tungsten carbide. A grinding operation is made with an abrasive diamond wheel to reduce the thickness. Then, small inserts are cut from the plates and brazed a second time by electromagnetic induction on the tool. The study takes place during the first brazing of alumina

plates, and after the cutting and grinding of the cutting inserts. It is a task of improvement to reduce residual stress that could lead to the deterioration of the cutting edge. The residual stress could consequently initiate and promote crack growth in the ceramic under technical loading in machining. The main purpose is to follow stress distribution of the submicron alumina through brazing and grinding. Different non-destructive methods for stress measurements are used to illustrate and review this issue. Firstly, by relying on the work from Ref 8 and Ref 9 in order to evaluate the residual stress at the interface, which has been assessed from an analytical model. The first objective is to propose an improvement of the model by using a strain-temperature equation computed from the difference of CTE of submicron alumina and tungsten carbide. For this purpose, the model takes into account the evolution of the Young's Modulus and the CTE according to the temperature. Then, the finite element method (FEM) has been used to compare the results to simulate stress in the bulk of the assembly. X-ray diffraction (XRD) measurements correlated with $\sin^2(\Psi)$ method, detailed by Ref 10, and indentation fracture method (IFM) on sub- μm alumina have also been used to determine residual stress in the ground surface. The investigations were aimed at summarizing residual stress state in submicron alumina, and suggest ways of improvements to reduce this latter.

2. Materials and Methods

2.1 Manufacturing of Ceramic Samples

2.1.1 Preparation of Materials. Aluminum oxide used in this work was prepared by an innovative liquid shaping method named Gelcasting (GC). After the burn out of organics at 800°C , ceramic is sintered in air followed by Hot Isostatic Pressing (HIP). The high-purity alumina produced by this low-defect process technology reaches homogeneous microstructure

T. Grunder, M. Bach, and P. Mille, LGeCo, INSA de Strasbourg, 24 Boulevard de la Victoire, 67084 Strasbourg, France; and A. Piquerez, Diamonde, 4 rue de Bruxelles, 67560 Marlenheim, France. Contact e-mail: timothee.grunder@gmail.com.

and high density. The substrates used for brazing were plates of sintered cobalt-cemented tungsten carbide provided by CER-ATIZIT under the reference CTE60A. The powders were densified by Cold Isostatic Pressing (CIP). The WC-Co has a volumic mass of $\rho_{wc} = 12.75 \text{ g/cm}^3$, a Young's modulus of $E = 450 \text{ GPa}$, and a fracture toughness of $K_{Ic} = 27 \text{ MPa}\sqrt{m}$. The traverse rupture strength is 2100 MPa , and the compressive strength is 3100 MPa . All the properties can be found in the supplier's generic handbook data, more specifically in its catalog entitled "Wear Parts."

2.1.2 Characterization. Density values for alumina were calculated by Archimedes's method. The Young's modulus was measured by resonance frequency by *Grindsonic*, according to EN 843-2. 4-point bending tests were done with 12 samples of $3 \times 4 \times 50 \text{ mm}^3$, regarding the ISO DIN 3327. The critical stress intensity factor K_{Ic} has been taken from SEVNB notching tests made with 8 bending bars of $3 \times 4 \times 50 \text{ mm}^3$ (DIN 14425-5), and hardness by 10 Vickers indentations with a 10 kg testing load (EN 843-4). Alumina's Young's modulus was defined from Ref 11 and tungsten carbide from Ref 12. Samples for IFM were polished with different diamond grit sizes provided by *Struers*. The inserts were polished with P180 for 5 min. The operation took place for 10 minutes with grit 220, 500, 1200, 2000, and finishing with a 1- μm diamond paste.

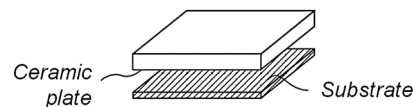
2.1.3 Brazing Process. The brazing plates need to have a high flatness with a low arithmetic roughness. These parameters are important for the plates positioning, to ensure bonding homogeneity. The latter was measured by STIL station with an optical sensor CHR 150. An area of $2 \times 2 \text{ mm}^2$ was swept, with a 2- μm sampling and 150- μm focal field depth. Plates were controlled after ultrasonic cleaning. An arithmetic roughness of $R_a = 0.361 \mu\text{m}$ was measured on the external surface of alumina before brazing. The joining of ceramic to WC-Co was done in a vacuum furnace (5-10 mbar) with a 50- μm thickness 72Ag-Cu filler. The eutectic temperature of the alloy was $780 \text{ }^\circ\text{C}$. Titanium hydride paste was applied to the face of the plates to enhance wettability of alumina. The cooling starts from 780 to $750 \text{ }^\circ\text{C}$ at a cooling speed of 15 K/min and from 750 to $20 \text{ }^\circ\text{C}$ at 4 K/min .

2.1.4 Grinding Process. A synthesis of the global manufacturing is proposed in Fig. 1. The first step is the high-temperature brazing of plates. Following the first step, ceramic plates of $100 \times 100 \times 3 \text{ mm}^3$ were used, and cut in inserts of $9 \times 4 \text{ mm}^2$ after the brazing. The plates were ground to a final thickness of 1.5 mm , and the WC-Co to 0.5 mm . The operation was performed with a resin-bonded wheel with a grit size of $60 \mu\text{m}$. The cut of small tooling inserts was performed with a diamond disk. After the third step, the inserts are ready to be brazed on the tool's body by an electromagnetic induction heating process. A Walter Helitronic Power peripheral grinding center was used to machine the outer surface of ceramic plates after the joining of the inserts on the tool. The cutting speed was 20 m/s , at a feed of 20 mm/min , with a 6- μm -grit-size grinding wheel. The thus produced cutting edge has a low surface roughness ($R_a \approx 0.3 \mu\text{m}$) and a sharp cutting edge ($< 5 \mu\text{m}$), that is required for the machining of wood-based materials.

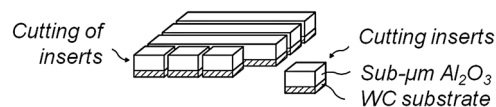
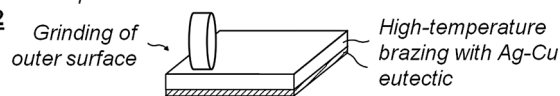
2.2 Characterization of the Brazing Interface and the Residual Stresses

Environmental Scanning Electron Microscopy (ESEM, Philip XL 30) was performed to observe the brazed interface between alumina and WC-Co. Energy dispersive x-ray spec-

Step 1



Step 2



Step 3

Second brazing at low-temperature on the cutting tool

Fig. 1 Manufacturing process of brazed cutting inserts

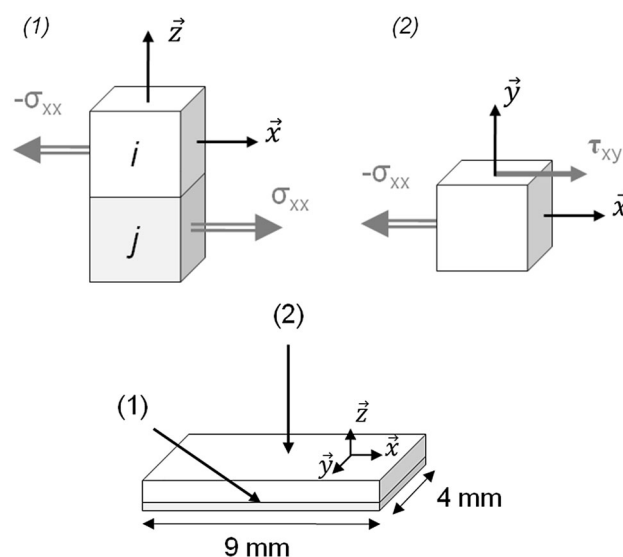


Fig. 2 Zone of residual stress measurements; (1) Biaxial stress at the brazing interface, (2) Stresses on the external surface

troscopy (EDX) analyses were used to obtain the cartography of chemical elements.

Residual stress has been determined in the brazing zone and in the external surface, as illustrated in Fig. 2. The analytical calculation and the FEM were performed at the interface (1), whereas x-ray analysis and IFM were done on zone (2). The analytical calculation was made to evaluate stress at the bonding interface, determined from the difference of CTE curves. The thermal expansion measurements were carried out using $3 \times 3 \times 40 \text{ mm}^2$ samples. Each specimen was introduced in a silica tube and put in a furnace. The displacement was recorded by a MECI system (B50545), using a mechanical feeler (B47948). Data were taped on a plotting table.

For the numerical approach, the calculation was done with MARC MENTAT. The meshing has been made with 50 000 hexahedral elements in $100 \times 100 \text{ mm}^2$ and 3-mm-thick plates. The Young's modulus and the CTE were defined as a function of temperature, in the same way that for the analytical calculation. Simulation results were obtained for a cooling

from 810 to 20 °C using the real cooling process parameters. X-ray stress analysis has been done with BRUKER Advance 8.8, where stresses were calculated with the $\sin^2(\Psi)$ method. The Pearson VII function has been used to model the diffraction peak profile. Values for alumina crystal structure were taken from Ref 13. A copper tube $\text{CuK}\alpha_1 = 0.1541$ nm was used to target the $2\theta = 136.07^\circ$ peak. The highest the diffraction angle is, the more the x-ray stress measurements are accurate. It is due to the amplification of the variation of interplanar distance at high angles. Deformation was calculated from the (146) plan, with $d = 1.37401$, in accordance with recommendations of Ref 19 for measurement on high-purity alumina. The inclination angle ψ varies from $[-45^\circ; 45^\circ]$, and the azimuth Φ from $[-45^\circ; 0^\circ; 45^\circ]$. Elastic constants used were $S_1 = -5.750 \times 10^{-7}$ and $\frac{1}{2}S_2 = 3.075 \times 10^{-6}$ with a Poisson ratio of 0.23. The x-ray depth penetration is about 14–20 μm under the surface. Global stress is determined from an addition of average stress values through the thickness. For the IFM, the measurements were made 4 times at different zone on the surface of the brazed samples. The cracks' length was measured using ESEM.

3. Results and Discussion

3.1 Mechanical Properties

The properties of submicron alumina after the GC and the HIP have been measured by the methods explained in section 2.1.2, and results are given hereinbelow. The volumic

mass for alumina made by GC is 3.98 g/cm^3 , its Young's modulus is 400 GPa, and the bending strength is $661 \text{ MPa} \pm 100 \text{ MPa}$. The fracture toughness is $K_{Ic} = 3.6 \pm 0.3 \text{ MPa} \sqrt{m}$, and the Vickers hardness is $2009 \text{ HV}10 \pm 20$. The average grain size estimated by the intercept linear method is $0.81 \mu\text{m}$.

3.2 Chemical Characterization of the Brazing Interface

The EDX shown on Fig. 3 depicts chemical distribution of elements through the brazing joint. At the top of the image at the gray image, alumina is at the top, and tungsten carbide at the bottom. The presence of aluminum, titanium, and tungsten confirms a good atomic migration by diffusion. Titanium has made a barrier at the interface with aluminum and oxygen. The formation of titanium oxide layer at the interfaces is a major point leading to the bonding of joint with ceramic and with the substrate. Quality of the brazing assembly is a function of oxidation degree according to Ref 14. Element cartography shows the success of the brazing operation regarding diffusion that leads to an optimal bonding between materials. The shear strength of the solder is given by the filler manufacturer of 180 MPa, but Ref 15 shows that with a reaction-thickness layer of 0.8 mm, the value is around 100 MPa. The microstructure of the layer is mainly a function of temperature and time of the brazing parameters.

3.3 Residual Stress at the Bonding Interface

Results from dilatometry tests are shown in Fig. 4. As shown hereinafter, Al_2O_3 has lower thermal expansion than

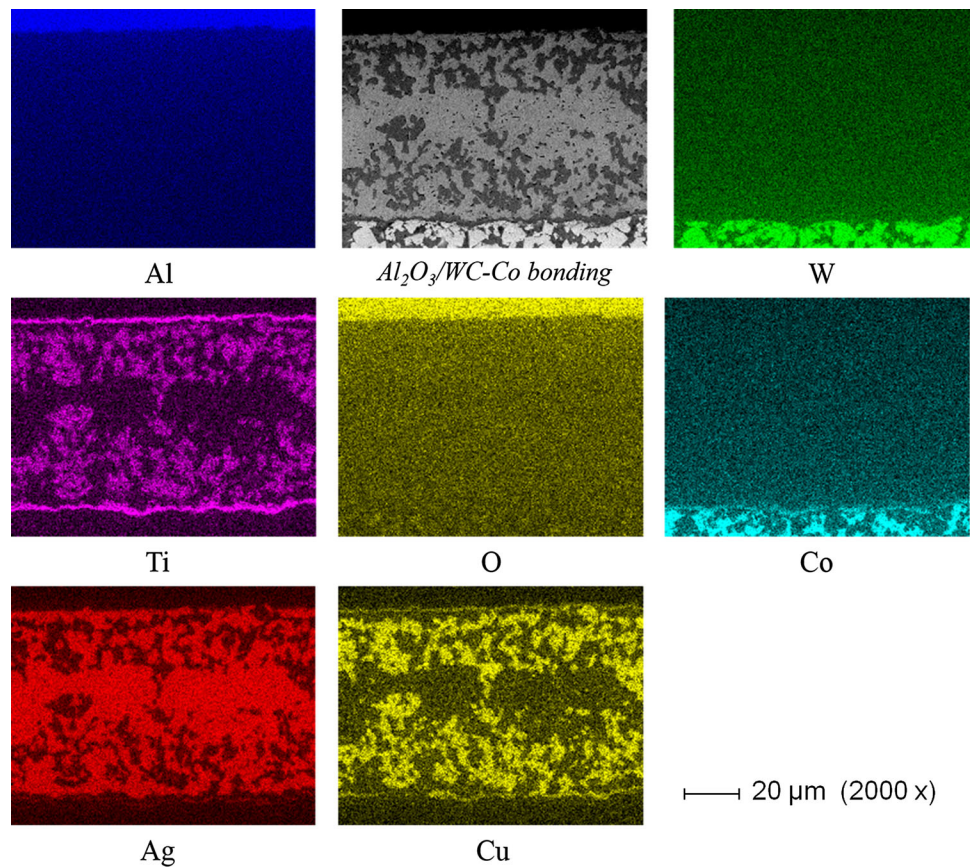


Fig. 3 EDS composition maps of the brazing interface $\text{Al}_2\text{O}_3/\text{WC-Co}$ with a Ag-Cu filler

WC. Variation of dilatation l in function of temperature θ is the so-called coefficient of thermal expansion α_L (CTE), expressed on its linear form at a constant pressure p by the relation

$$\alpha_L = \frac{1}{l_0} \left(\frac{dl}{d\theta} \right)_p \quad (\text{Eq 1})$$

The CTE of each material has been determined from the plotted curves related to Fig. 4. Usually, a linear form is commonly accepted on a temperature range. Nevertheless, a polynomial function is more appropriate here. In our results, a polynomial of the third degree gives the highest coefficient of determination ($R^2 \approx 1$). As a consequence, the CTE of both materials takes the form of a second-degree polynomial.

Difference in thermal dilatation ensures stress at the interface during the cooling. Strain ε due to mismatch caused by the difference in variation of thermal expansion coefficients follow the form:

$$\varepsilon = (\alpha_{al} - \alpha_{wc}) \Delta\theta \quad (\text{Eq 2})$$

where $\Delta\theta$ represents the difference in temperature between the bonding temperature θ_e (at the eutectic point) and the room temperature θ_{RT} . However, to obtain a more accurate strain evolution, it is possible to integrate Eq 2 after having written the CTE in their developed form, as exhibited in Eq 1. Then, we obtain the strain evolution in function of tem-

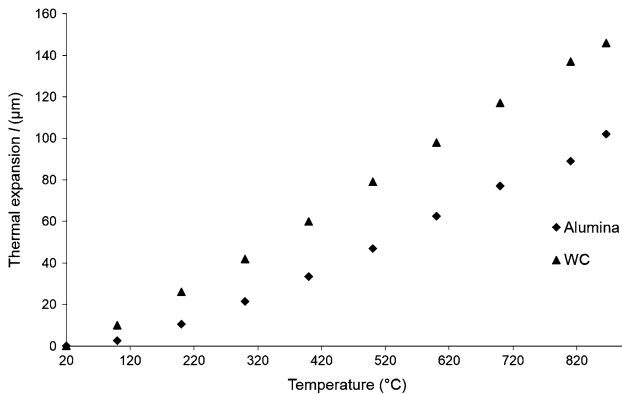


Fig. 4 Evolution of thermal expansion of coupled materials

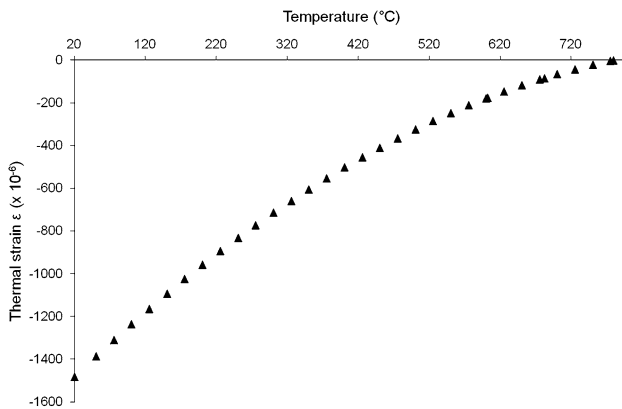


Fig. 5 Strain evolution at the brazing interface of sub- μm Al_2O_3

perature, as shown in Fig. 5. Maximal strain is reached when the cooling ends at 20 °C. The resulted strain is negative because alumina CTE is lower than that of tungsten carbide.

Stress calculation model presented hereinafter in Eq 3 was initially introduced by Ref 16, and resumed by Ref 8. It roughly defines stress σ_{xx} at the interface between two bonded materials i and j , regarding the fact that materials can deform elastically only (an acceptable hypothesis for ceramic). In Eq 3, the model could be improved by incorporating the Young's Modulus E and thermal expansion $dl/d\theta$, both being a function of temperature. Stress at the interface σ_{xx} could be calculated by integration difference in thermal expansion (from Eq 1) from eutectic temperature θ_e to room temperature θ_{RT} , as follows:

$$\sigma_{xx}(\theta) = \frac{E_i(\theta) \cdot E_j(\theta)}{E_i(\theta) + E_j(\theta)} \cdot \int_{\theta_e}^{\theta_{RT}} \left[\frac{1}{l_{0i}} \left(\frac{dl_i}{d\theta} \right) - \frac{1}{l_{0j}} \left(\frac{dl_j}{d\theta} \right) \right] d\theta \quad (\text{Eq 3})$$

Figure 6 relates residual stress at the interface of pure Al_2O_3 and WC-Co. The results are valid for a material volume close to the bonded interface. The maximal value is 300 MPa at room temperature. The ceramic is under a compressive stress. In this approach, the role of the brazing joint was neglected. Nevertheless, it strongly contributes to absorb plastically a part of strain and contribute to relax residual stress (Ref 6-9). This model offers the possibility to reduce stress by improving the fit between the curves of thermal expansion (Fig. 4), instead of using fix CTE values usually given for a temperature range. It could also give the possibility for some ceramic-substrate-brazed assembly to quantify the stress induced by an allotropic transformation during the cooling. For example, the brazing of a 3Y-ZrO_2 to C45 assembly takes place at 800 °C, and generates a change in crystallographic structure of steel that leads to a brutal variation of stress. Initially, 3Y-ZrO_2 ceramic was compressed until 682 °C, and then the stress changes in tensile stress. When the temperature reaches 602 °C, it comes back in compressive stress. This phenomenon could be responsible for some localized lack of adhesive bonding and failure of the ceramic. In order to design the brazing of an assembly, dilatometry measurements allied to this analytical model could be used.

3.4 Residual Stress Simulated Using the Finite Element Method (FEM)

The purpose of the following investigation is to get a view on stress distribution on bulk materials. The meshing has been made with plates in ceramic and tungsten carbide of the same

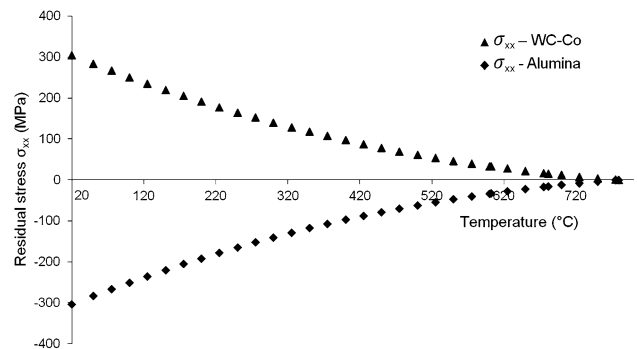
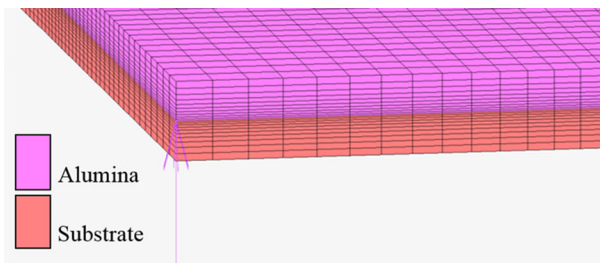
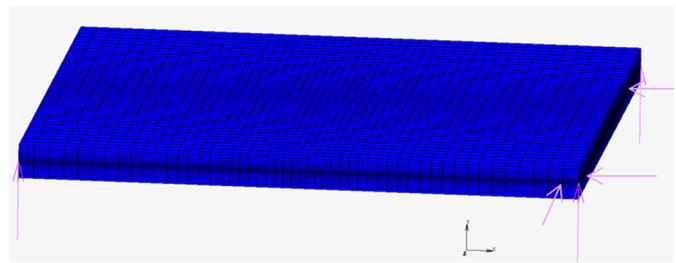


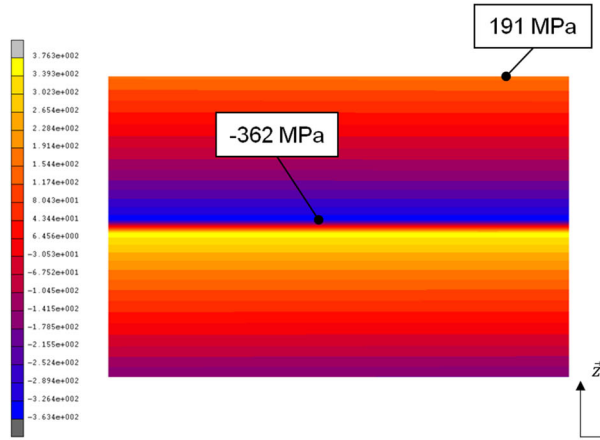
Fig. 6 Residual stress evolution at the brazing interface calculated from the measurement of difference in CTE



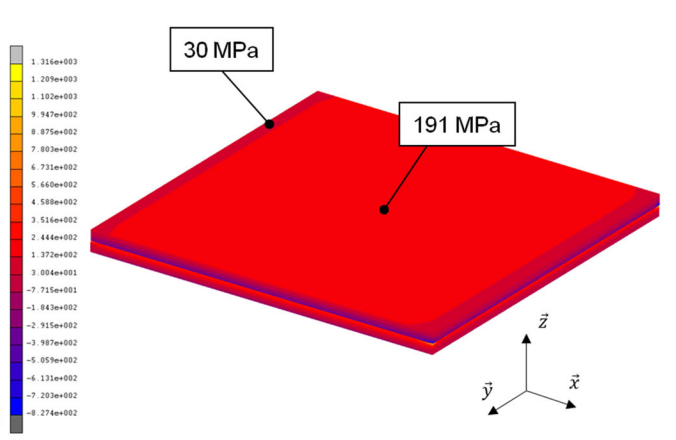
Modeling the distribution of the elements



Conditions of constrain of ceramic-substrate plates



Stress distribution at the bonded interface



Stress on the assembled plates after cooling, at room temperature

Fig. 7 Simulation of residual stress σ_{xx} after cooling at room temperature on alumina-WC-Co-brazed assembly calculated by FEM on MARC MENTAT

dimensions. Alumina elastic modulus function was calculated from Ref 11 and the CTE α_{al} and α_{wc} were taken from the dilatometer measurements. For WC-Co substrate, $E_{wc}(\theta)$ was taken from Ref 12, and the volumic mass value used was $\rho_{wc} = 12.75 \text{ g/cm}^3$. The graphs depicted in Fig. 7 and 8 show numerical results of residual stress simulations. As shown on Fig. 7, ceramic is under a compressive stress of -362 MPa. No significant stress was found in the normal direction (\vec{z}). Stress on the outer surface is 200 MPa. However, this model does not take into account the shear stress that arises in the interface. According to Ref 15, shear strength of the bonding joint is dependent on kinetic growth of reaction layer. Stress evolutions are close to the results determined analytically. Figure 9 revealed that there is a good qualitative degree of agreement between analytical and FEM results.

Similar stress configuration in the assembly was found by Ref 17. It relates compressive stress in a Si_3N_4 -steel brazing assembly. The author puts forward the hypothesis that compressive stress in ceramic is major than shearing stress. Charreyron's Ref 9 introduced different models of stress calculation at the interface with the modelization of different bonding joints. The latter model is noticeably different that the one submitted hereinabove because of the shearing stress taken into account in the joint. The shape of the brazing assembly has an influence on residual stress distribution, as shown by Ref 18. Stress modes are different in the bulk of ceramic and its substrate than at the bonding interface. Moreover, stress intensity on the external surface decreases with the augmentation of the thickness of the assembly.

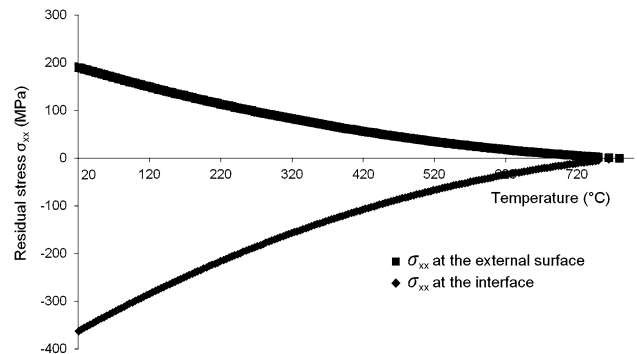


Fig. 8 Residual stress evolution σ_{xx} at the opposite surfaces during the cooling of alumina-tungsten carbide assembly

3.5 Residual Stress on the Outer Surface by X-ray Measurements

Results shown in Fig. 10 highlight residual triaxial stress after the brazing and the cut of small insert (a). The principal stresses σ_I and σ_{II} are, respectively, 103.2 MPa, is 66.2 MPa, and σ_{III} is 41.6 MPa. The shear stress is $\tau_{xy} = -27.0 \text{ MPa}$. Error tolerance on values is between 6 and 8%. After the grinding (b), stress mainly becomes biaxial ($\sigma_{III} = -4.5 \text{ MPa}$). Then, main stresses become $\sigma_I = 128.1 \text{ MPa}$ and $\sigma_{II} = 94.9 \text{ MPa}$. The shear stress decreased at -20.1 MPa .

By using this method, a view of the average stress state of the center of the samples is possible. The stress decreases after

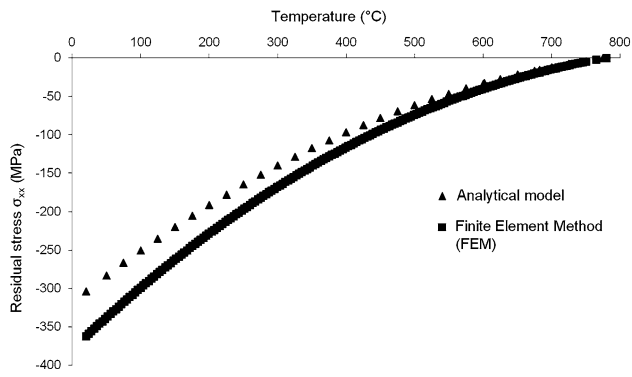


Fig. 9 Comparison of stress evolutions between the models determined by the analytical approach and the FEM

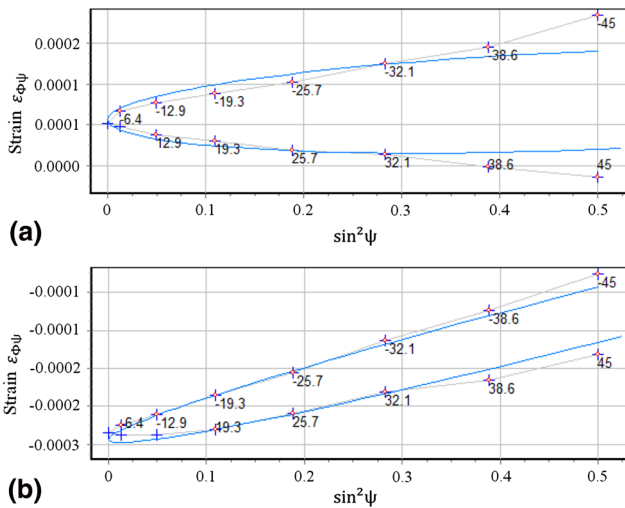


Fig. 10 Residual microstrain $\epsilon_{\phi\psi}$ between ψ $[-45^\circ;45^\circ]$ on the external face, after brazing at $\Phi = 0^\circ$ (a), and after brazing and grinding at $\Phi = -45^\circ$ (b)

the cutting of small inserts, and becomes mainly longitudinal. The surface stress state of post-sintered submicron alumina was investigated by Ref 20. The results suggest a residual stress around 20-30 MPa mainly due to grains thermal expansion anisotropy. Here, the presence of shear stress could generate dislocation

3.6 Residual Stress by Indentation Fracture Method (IFM)

Indentation in fragile material results in cracking at the tip of plastic zone. This method shows the evolution of stress over the surface of the inserts. After the brazing, the residual stress generates longer cracks. Difference between crack length between a stress-free state and a residual stress state indicates residual stress intensity. At the center of the stress curves in Fig. 11, the middle point is made at the center of the sample. Additionally, 2 points were printed from both sides, in width and lengthwise. As a result, stress in the two main directions at the external surface was estimated.

The Ref 21 showed that residual stress in brittle material could be approached by IFM which resulted from the measurement of the crack length generated at the corner of the indentation print. Then the residual stress could be determined by the following formula (Eq 4):

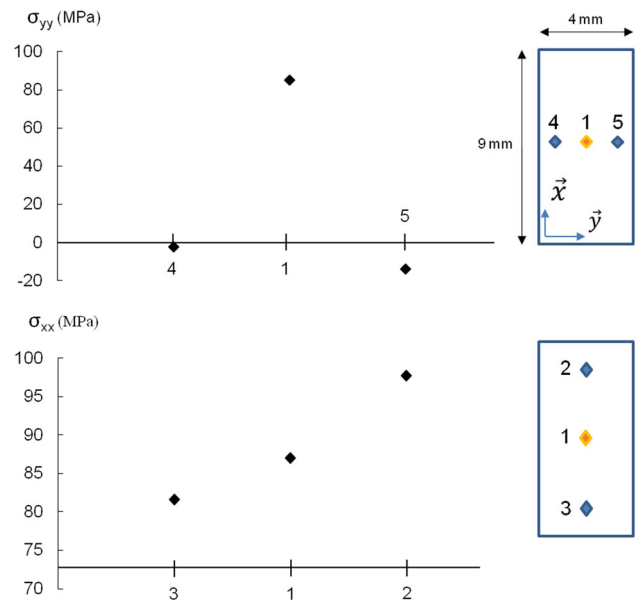


Fig. 11 Residual stress distribution through external surface of 9×4 alumina-WC brazing assembly

$$\sigma_r = \left[\frac{K_{Ic}}{(\pi \cdot c \cdot \Omega)^{1/2}} \right] \cdot \left[1 - \left(\frac{c_0}{c} \right)^{3/2} \right] \quad (\text{Eq 4})$$

Initially, the crack length c_0 in stress-free corundum was measured. According to the indentation geometry, $\Omega = \frac{4}{\pi^2}$ has been used, as recommended by Ref 22. Regarding previous results, lower residual stress was found. The σ_{yy} stress appeared to be almost near from zero at the surface edges (points 4 and 5), and of 87 MPa in the middle. Residual stress decreases in the small inserts, after the cut of big plates. The cutting and the grinding of inserts have relaxed stress, and no grain size effects are expected here, where the values agree with the XRD stress measurements. As a conclusion, IFM fits for the characterization of the residual stress in submicron alumina. The reduction of the crystallite size does not affect the crack length at the indentation corner, and the use of Eq 4 gives coherent results.

3.7 Fracture and Damage

As shown in Fig. 12, difference in CTE between alumina and tungsten carbide could generate crack. The use of tungsten carbide composite with lower cobalt content increased interfacial stress and have led to failure. In this study, the WC-Co used has more than 25 wt.% of cobalt. Titanium oxide layer (from green arrows) could be observed. The residual stress could have propagated a crack from an initial weakness or from a defect (e.g., lack of bonding, microcrack, or porosity). The cracks could also start from a junction (Ref 23).

Micrograph in Fig. 13 shows the damaged surface after being ground. The outer surface (on Fig. 13) is expected to be used as a wear part for the machining of abrasive materials, such as wood-based products. In this context, it is essential to prevent defects formation which would cause a decrease on the global strength of ceramics. In an abrasive wear mode, the smaller the defects are on the rake face, the longer the tool's lifetime is Ref 7-25. The residual stress needs to be estimated regarding the manufacturing of ceramic cutting tools, as the

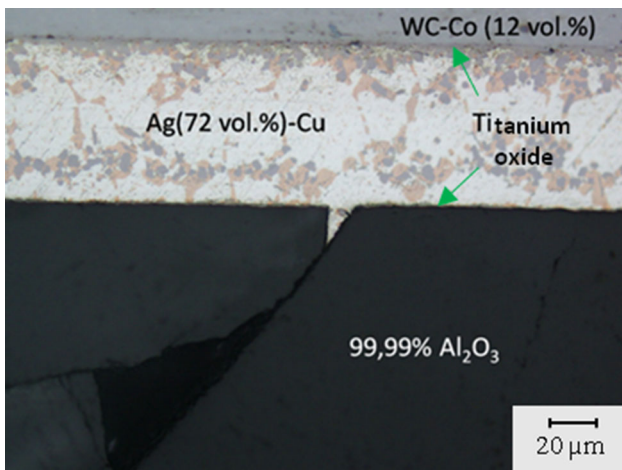


Fig. 12 Crack at the interface of alumina-WC-Co brazed interface

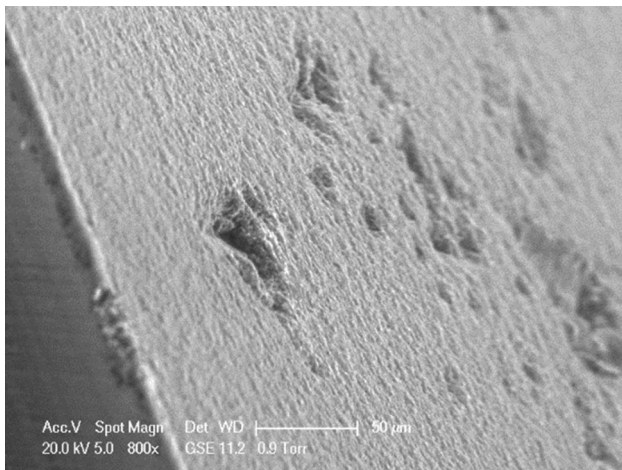


Fig. 13 Material pull-out after grinding, promoted by residual stress on external surface

compressive stress could increase the wear resistance, whereas the shear stress can reduce the critical stress value needed to activate a dislocation movement within the crystallite lattice (Ref 24). The material loss observed on Fig. 13 has been initiated by the global stress that results from the manufacturing process. The local shear stress generated by the grinding has contributed to the microcracking as well. Then, subcritical crack growth in the ceramic has generated material pull-out. The less amount of stress is induced in the processes, the less damaged assembly is obtained.

4. Conclusions

The manufacturing of pure submicron grain size alumina by gelcasting has led to a highly wear-resistant material for cutting tools. The high bending strength and the hardness make the ceramic difficult to braze and to grind.

Different processes have been used to quantify the residual stress after the bonding of alumina with tungsten carbide and the grinding with abrasive wheel. An improved equation has been proposed for the calculation of the residual stress at the

interface in order to estimate the variation of strain and stress during the cooling cycle of the bonded materials. The new model takes into account the evolution of the Young's Modulus and the CTE in accordance with the temperature, and could be used to reduce the residual strain. The calculation could be employed to follow the prompt variation of stress induced by an allotropic change in the case of a bonding with a steel substrate. The estimated residual stress at the close vicinity of submicron alumina and tungsten carbide brazing area exhibits a qualitative degree of agreement with the FEM calculation.

The stress state at the outer surface of the ceramic cutting parts after brazing and grinding has been investigated by XRD and IFM. Both results concurred and indicated that it is mainly tensile and shear stresses that appeared in the crystallites lattices of submicron alumina. The mechanical stress is wider in the middle and becomes smaller to the edges. The induced residual stresses have influenced the integrity of the brazing materials by promoting material pull-out. The proposed methods enable to determine the brazing and grinding residual stress state for submicron alumina cutting inserts.

Acknowledgment

Thanks to J. Klimke and A. Krell of IKTS Fraunhofer institute for the manufacturing and the mechanical characterization of the submicron alumina. Our gratitude to J. Krier and G. Schuhler for running all the simulations by FEM. The author would also thank PNL INNOTECH for having achieved the brazing in high temperature. This work was supported by the French National Association for Research and Technology (ANRT) under Contract No. 2011/1171.

References

1. H. Chen, L. Li, R. Kemps, B. Michielsens, M. Jacobs, F. Sniijkers, and V. Middelkoop, Reactive Air Brazing for Sealing Mixed Ionic Electronic Conducting Hollow Fibre Membranes, *Acta Mater.*, 2015, **88**, p 74–82
2. C. Walker, J. Romero, and R. Stokes, Active-Brazed Ceramic-Tungsten Carbide Assemblies for Seal Applications, *Microsc. Microanal.*, 2011, **17**, p 1844–1845
3. K. Scott-Weil, C.A. Coyle, J.T. Darsell, G.G. Xia, and J.S. Hardy, Effects of Thermal Cycling and Thermal Aging on the Hermeticity and Strength of Silver–Copper Oxide Air-Brazed Seals, *J. Power Sources*, 2005, **152**, p 97–104
4. A. Krell, P. Blank, H. Ma, T. Hutzler, and M. Nebelung, Processing of High-Density Submicrometer Al_2O_3 for New Applications, *J. Am. Ceram. Soc.*, 2003, **86**, p 546–553
5. J.-W. Park, P.F. Mendez, and T.W. Eagar, Strain Energy Distribution in Ceramic-to-Metal Joints, *Acta Mater.*, 2002, **50**, p 883–899
6. J.-W. Park, P.F. Mendez, and T.W. Eagar, Strain Energy Release in Ceramic-to-Metal Joints by Ductile Metal Interlayers, *Scr. Mater.*, 2005, **53**, p 857–861
7. T. Grunder, "Contribution to the Application of Submicron Al_2O_3 and 3Y-ZrO_2 Ceramics to the Machining of Wood-Based Materials," Ph.D. thesis, 2015 (In French)
8. O.M. Akselsen, Advances in Brazing of Ceramics, *J. Mater. Sci.*, 1992, **27**, p 1989–2000
9. P.O. Charreyron, D.O. Patten, and B.J. Miller, Modeling of Ceramic to Metal Brazed Joints, *Proc. Int. Forum Struct. Ceram. Join. Ceram. Eng. Sci. Proc.*, 1989, p. 1801–1824
10. B. Eigenmann, B. Scholtes, and E. Macherauch, Determination of Residual Stresses in Ceramics and Ceramic-Metal Composites by X-ray Diffraction Methods, *Mater. Sci. Eng. A*, 1989, **118**, p 1–17

11. W. Pabst and E. Gregorová, Isothermal and Adiabatic Young's Moduli of Alumina and Zirconia Ceramics at Elevated Temperatures, *J. Eur. Ceram. Soc.*, 2013, **33**, p 3085–3093
12. V.T. Golovchan, On the Thermal Residual Microstresses in WC–Co Hard Metals, *Int. J. Refract. Met. Hard Mater.*, 2007, **25**, p 341–344
13. D.M. Toebbens, N. Stuesser, K. Knorr, H.M. Mayer, and G. Lampert, Calculated from ICSD using POWD-12+, *Mater. Sci. Forum*, 2001, **378**, p 288
14. R.M. Do Nascimento, A.E. Martinelli, A.J.D.A. Buschinelli, and A.N. Klein, Brazing Al₂O₃ to Sintered Fe-Ni-Co Alloys, *J. Mater. Sci.*, 1999, **34**, p 5839–5845
15. T. Torvund, Ø. Grong, O. Akselsen, and J. Ulvensoen, A Process Model for Active Brazing of Ceramics: Part II, Optimization of Brazing Conditions and Joint Properties, *J. Mater. Sci.*, 1997, **32**, p 4437–4442
16. X.S. Ning, T. Okamoto, Y. Miyamoto, A. Koreeda, and K. Suganuma, Effect of Oxide Additive in Silicon Nitride on Interfacial Structure and Strength of Silicon Nitride Joints Brazed with Aluminium, *J. Mater. Sci.*, 1989, **24**, p 2865–2870
17. K. Suganuma, T. Okamoto, M. Koizumi, and M. Shimada, Effect of Thickness on Direct Bonding of Silicon Nitride to Steel, *J. Am. Ceram. Soc.*, 1985, **68**, p 334–335
18. K. Suganuma, T. Okamoto, M. Koizumi, and K. Kamachi, Influence of Shape and Size on Residual Stress in Ceramic/Metal Joining, *J. Mater. Sci.*, 1987, **22**, p 3561–3565
19. K. Tanaka, Y. Yamamoto, and K. Suzuki, Elastic Constants of Ceramics for X-Ray Residual Stress Measurement, in *Int. Conf. Residual Stress.*, 1989, p 328–334
20. A. Krell, A. Teresiak, and D. Schläfer, Grain Size Dependent Residual Microstresses in Submicron Al₂O₃ and ZrO₂, *J. Eur. Ceram. Soc.*, 1996, **16**, p 803–811
21. D.B. Marshall and B.R. Lawn, An Indentation Technique for Measuring Stresses in Tempered Glass Surfaces, *J. Am. Ceram. Soc.*, 1977, **60**, p 86–87
22. D.B. Marshall and B.R. Lawn, Residual Stress Effects in Sharp Contact Cracking: I, *J. Mater. Sci.*, 1979, **14**, p 2001–2012
23. V. Cazajus, Numerical and Experimental Approach of Ceramic-Metal bonding made by Brazing for the Creation of a Design, Polytechnic National Institute of Toulouse, 2007 (In French)
24. C. Noyan, and J.B. Cohen, Residual Stress—Measurement by Diffraction and Interpretation, *Materials Research and Engineering*, 1987, Springer New York
25. A. Krell, Improved Hardness and Hierarchic Influences on Wear in Submicron Sintered Alumina, *Mater. Sci. Eng.: A*, 1996, **209**, p 156–163